

# Recent elevation changes on the ice streams and ridges of the Ross Embayment from ICESat crossovers

Benjamin E. Smith

Earth and Space Sciences, University of Washington, Seattle, Washington, USA

Charles R. Bentley

Department of Geology and Geophysics, University of Wisconsin, Madison, Wisconsin, USA

Charles F. Raymond

Earth and Space Sciences, University of Washington, Seattle, Washington, USA

Received 10 August 2005; accepted 13 September 2005; published 14 October 2005.

[1] We analyze differences in ICESat elevation estimates at orbital crossover locations to determine short-term rates of elevation change for small regions within the Ross Embayment of the West Antarctic Ice sheet. A linear regression of crossover elevation difference against time difference gives an estimate of the mean elevation-change rate during the ICESat mission to date. We observe prevalent elevation change in the south, with uplift in the upstream end of Kamb Ice Stream at  $0.24\text{--}0.30\text{ m a}^{-1}$ , and thinning in the parts of Whillans Ice Stream, Mercer Ice Stream, and the adjacent Conway and Engelhardt ice ridges at  $0.05\text{--}0.18\text{ m a}^{-1}$ . These rates of elevation change are too large to be explained by the  $0.02\text{--}0.03\text{ m a}^{-1}$  formal regression error, by seasonal height variations, or by accumulation- or densification-rate variability, suggesting that they reflect real variations stemming from ice dynamics of the region. **Citation:** Smith, B. E., C. R. Bentley, and C. F. Raymond (2005), Recent elevation changes on the ice streams and ridges of the Ross Embayment from ICESat crossovers, *Geophys. Res. Lett.*, 32, L21S09, doi:10.1029/2005GL024365.

## 1. Introduction

[2] NASA's Ice, Cloud and land Elevation Satellite (ICESat) mission carries Earth's first polar-orbiting satellite laser altimeter Geoscience Laser Altimeter System (GLAS). The 86S orbit extent provides first-time altimetric coverage of the southern parts of the Ross Ice Shelf. By mid 2005, ICESat had collected ice-surface-elevation data over a period of just more than 24 months, allowing resolution of cm-per-year elevation changes (R. Schutz et al., ICESat mission overview, 2005, submitted to *Geophysical Research Letters*, 2005).

[3] Recent studies of the ice dynamics of the Ross Embayment (RE), near the southern limit of ICESat coverage between  $75^{\circ}\text{S}$  and  $86^{\circ}\text{S}$ , show large rates of change in ice velocities and local mass balance over decadal and shorter time scales. A general review of WAIS changes has been given by *Alley and Bindshadler* [2001]. GPS-based point measurements coupled with airborne laser altimetry surveys show rapid thickening in the upper trunk of KIS (Kamb Ice Stream, further abbreviations defined in

Table 2), rapid thinning in the upper trunk of WIS, and near balance in the catchment region of WIS [*Spikes et al.*, 2003]. This is consistent with velocity changes recently observed in the ice streams: The stagnation of KIS produced a net thickening in the region where flow from the still-active tributaries flows into the stagnant trunk region [*Price et al.*, 2001]. Likewise, the downstream region of WIS has slowed faster than the upstream region, which could lead to thickening of the middle of the ice stream [*Joughin et al.*, 2002], although WIS as a whole is largely in balance [*Joughin and Tulaczyk*, 2002]. The spatial pattern of long-term relative elevation change across the RE was estimated from the shapes of internal layers in the inter-stream ridges, detected by ice penetrating radar. These show a gradient in thinning from south to north, with WIS thinning faster than BIS [*Nereson and Raymond*, 2001]. In this paper we use ICESat data to determine elevation changes in the RE. Although these elevation differences reflect time-varying snow deposition and densification as well as ice dynamics, we show that they now are adequate to demonstrate that the largest predicted changes are ongoing, and to suggest that rapid change is occurring in regions not covered by previous satellite altimeters.

## 2. Methods

[4] We recover rates of elevation change from analysis of elevation estimates at orbital crossover locations. We select a subset of the approximately 110,000 crossovers in the RE that we believe to have the smallest contamination by errors, and divide these into geographical regions to obtain the spatial distribution of elevation-rate estimates. We then solve for the mean rate of elevation change during the observation period by linear regression by including an estimate of the data-covariance matrix. Finally, we test the sensitivity of our recovered elevation-change rates to seasonal cycles in the surface elevation due to accumulation and time-varying densification.

[5] Throughout this paper we will measure data residuals using  $\hat{\sigma}$ , a robust estimator of the standard deviation.  $\hat{\sigma}$  is equal to half the width of the range that contains the central 68% of a distribution of residuals.

### 2.1. ICESat Data and Processing

[6] We combine data from the GLA01 Global Altimetry Data and GLA12 Ice Altimetry Data. The data versions

**Table 1.** GLA01 and GLA12 Versions and Dates for Laser Operations Periods

Ops Period	GLA01	GLA12	Dates
1	13	18	2/20/03–3/20/03
2a	19	21	9/25/03–11/18/03
2b	16	16	2/17/04–3/21/04
2c	17	17	5/18/04–6/21/04
3a	18	18	10/3/04–11/8/04
3b	19	19	2/18/05–3/24/05

used are the most current available in May 2005; dates and version numbers are listed in Table 1. We correct the return energy on GLA01 from all data from Release 21 and earlier using the formula given by *Fricker et al.* [2005]. We correct our data for detector saturation by shortening the range for all returns with a gain setting equal to 13 by 0.022 m/fJ for every fJ of return energy over 13.1 [*Sun et al.*, 2003].

[7] To minimize errors due to forward scattering by clouds and highly saturated returns, we filter the data based on a set of parameters describing the return pulse, provided in GLA12. Returns unaffected by saturation or forward scattering resemble narrow Gaussian pulses, similar to the transmitted pulse. We expect saturation and forward scattering to change the shape of these pulses, increasing the apparent surface roughness (estimated from the width of the return-pulse), the misfit between the return pulse a Gaussian, and expect clouds to decrease the apparent surface reflectivity. We also expect forward scattering to increase the apparent shot-to-shot surface roughness because of inhomogeneities in cloud layers. After some experimentation, we find that if we reject all returns for which the apparent surface reflectivity is less than 40% or the apparent surface roughness is more than 2 m or the RMS difference between the digitized waveform and the best-fitting single Gaussian is more than 0.06 mV, we can reduce the RMS shot-to-shot surface roughness for the flat parts of WAIS from 0.30 m to 0.025 m. These criteria reject about 45% of all shots. To remove the few remaining large outliers resulting from small-scale surface roughness, undetected forward scattering, and minor aberrations in the pulse-fitting routine, we use an iterative 3- $\sigma$  edit in calculating our regressions.

[8] We calculate cross-over differences by linear interpolation into the elevations on each track to find the elevations at the crossing point. We estimate that the errors introduced by this interpolation are less than 0.05 m, based on the RMS error in estimating the elevations of every second shot in our region from the remaining shots. This error is a small component of the other errors discussed in section 2.3.

## 2.2. Elevation Change Regions

[9] To obtain centimeter-level regression errors, at least a few hundred crossover measurements are required. Instead of dividing the ice sheet into a regular grid for this averaging, we prefer to make divisions based on our knowledge of the local glaciology [*Bentley*, 1987]. We divide the RE into 28 regions (Figure 1), defined by 5 ice stream trunks, 10 well-defined tributaries, and 4 inter-stream ridges. We make smaller subdivisions in a few important areas: e.g. we treat the upstream end of the trunk of KIS (Kamb Junction) separately from the stagnant

downstream end of KIS, and divide RIR into a slow-flowing section ( $RIR_W$ ; abutting Siple Dome), and an upstream section ( $RIR_E$ ) including some faster tributary flow. In the far south, the crossover density is very high, allowing the subdivision of MIS and CIR. We have also calculated elevation change rates for small areas surveyed by airborne laser altimetry; results from these areas are described by B. Csatho et al. (ICESat measurements confirm complex patterns of thickness changes on Siple Coast ice streams, Antarctica, submitted to *Geophysical Research Letters*, 2005, hereinafter referred to as Csatho et al., submitted manuscript, 2005).

## 2.3. Regression Process

[10] We assume that the elevation difference at each crossover results from a linear rate of elevation change,  $\dot{z}$ , that is constant for each local region of the ice sheet. This can be written as a matrix equation:

$$\mathbf{d} = \dot{z}\mathbf{t} + \boldsymbol{\varepsilon} \quad (1)$$

Here  $\mathbf{d}$  is a vector of  $N$  elevation differences,  $z_{ai} - z_{di}$ ,  $\mathbf{t}$  is a vector of  $N$  time differences, and  $\boldsymbol{\varepsilon}$  is a vector of errors.

[11] The least-squares  $\dot{z}$  estimate based on equation (1) is:

$$\dot{z} = (\mathbf{t}^T C^{-1} \mathbf{t})^{-1} \mathbf{t}^T C^{-1} \mathbf{d} \quad (2)$$

Here  $C$  is the  $N \times N$  data covariance matrix for errors in elevation measurements.  $(\mathbf{t}^T C^{-1} \mathbf{t})^{-1} \mathbf{t}^T$  is the generalized

**Table 2.** Rates of Elevation Change and Abbreviations for Regions of the Ice Sheet<sup>a</sup>

Region	Abbreviation	Elevation Rate	Season
Mercer IS W	$MIS_W$	$-0.02 \pm 0.02$	-0.01
Mercer IS M	$MIS_M$	$-0.04 \pm 0.02$	-0.06
Mercer IS E	$MIS_E$	$-0.05 \pm 0.02$	-0.08
Conway IR SW	$CIR_{SW}$	<b><math>-0.18 \pm 0.02</math></b>	-0.17
Conway IR SE	$CIR_{SE}$	<b><math>-0.13 \pm 0.02</math></b>	-0.14
Conway IR N	$CIR_N$	<b><math>-0.18 \pm 0.02</math></b>	-0.18
Whillans IS trunk	$WIS_{trunk}$	$0.06 \pm 0.02$	0.05
Whillans IS W	$WIS_W$	$0.05 \pm 0.02$	0.04
Van der Veen IS	$VdV$	<b><math>-0.16 \pm 0.02</math></b>	<b>-0.21</b>
Whillans IS N	$WIS_N$	<b><math>-0.15 \pm 0.02</math></b>	-0.17
Engelhardt IR S	$EIR_S$	<b><math>-0.12 \pm 0.02</math></b>	-0.13
Engelhardt IR N	$EIR_N$	<b><math>-0.10 \pm 0.02</math></b>	-0.11
Engelhardt IR E	$EIR_E$	$0.04 \pm 0.03$	0.03
Kamb IS trunk	$KIS_{trunk}$	<b><math>-0.06 \pm 0.02</math></b>	-0.08
Kamb IS junction	$KIS_{junc}$	<b><math>0.27 \pm 0.03</math></b>	0.28
Kamb IS S	$KIS_S$	<b><math>0.26 \pm 0.03</math></b>	0.20
Kamb IS N	$KIS_N$	<b><math>0.29 \pm 0.03</math></b>	0.23
Siple Dome	$Siple_{Dome}$	<b><math>-0.09 \pm 0.02</math></b>	-0.13
Raymond IR W	$RIR_W$	$0.01 \pm 0.03$	-0.01
Raymond IR E	$RIR_E$	<b><math>0.17 \pm 0.03</math></b>	0.14
Bindschadler IS tr.	$BIS_{trunk}$	<b><math>-0.18 \pm 0.03</math></b>	-0.22
Bindschadler IS S	$BIS_S$	$-0.07 \pm 0.08$	-0.10
Bindschadler IS N	$BIS_N$	<b><math>-0.09 \pm 0.03</math></b>	-0.11
Shabtaie IR	$SIR$	<b><math>-0.14 \pm 0.04</math></b>	-0.21
Macayea IS trunk	$MIS_{trunk}$	<b><math>-0.12 \pm 0.03</math></b>	-0.14
Macayea IS S	$MIS_S$	$-0.05 \pm 0.03$	-0.09
Macayea IS	$MIS_N$	$-0.02 \pm 0.05$	0.05
Harrison IR	$HIR$	$-0.02 \pm 0.04$	-0.08

<sup>a</sup>Column 3 gives the uncorrected elevation-change rate, shown in bold if significantly different from zero. Column 4 gives the elevation-change rate corrected for the season-cycle estimate. Regions may be designated IS: ice stream and IR: ice ridge.

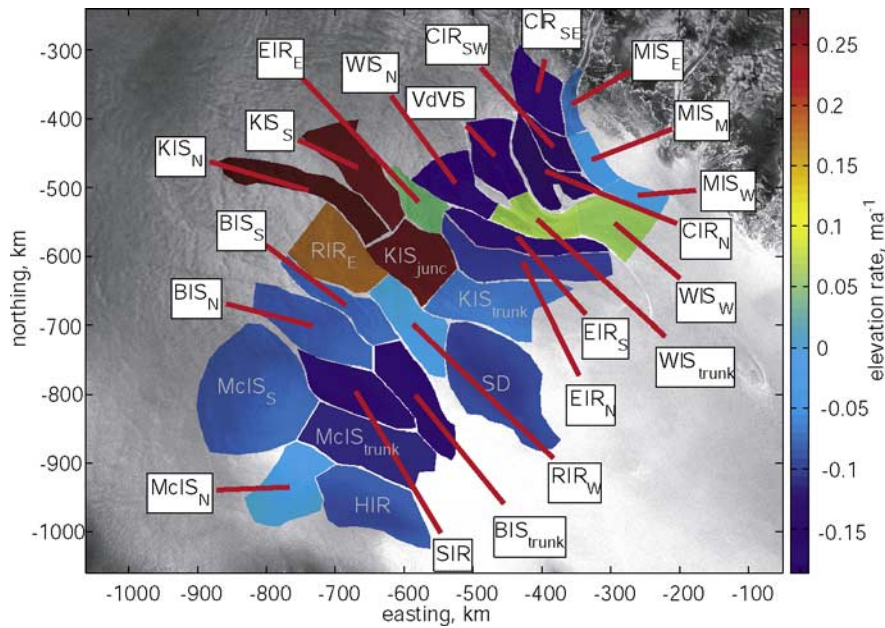


**Figure 1.** Derived rates of elevation change for the 28 regions of the RE used in this study, listed in Table 2. Background image is the RAMP mosaic [Jezek and RAMP Product Team, 2002].

inverse of  $\mathbf{t}$ , abbreviated  $\mathbf{t}^{-g}$ . The formal error estimate for  $\dot{z}$  is then [Menke, 1989]

$$\sigma_z^2 = \mathbf{t}^{-gT} \mathbf{C}^{-1} \mathbf{t}^{-g}. \quad (3)$$

[12] The data covariance matrix is constructed as:

$$C_{ij} = \begin{cases} \sigma_{pass}^2 + \sigma_{shot}^2 & i = j \\ (1/2)\sigma_{pass}^2 & i \text{ and } j \text{ from same pass} \\ 0 & \text{otherwise.} \end{cases} \quad (4)$$

Here  $\sigma_{pass}$  is the error in  $z$  that is consistent for each pass over a region, while  $\sigma_{shot}$  is the error in  $z$  that is uncorrelated from shot to shot. The covariance matrix is necessary for accurate estimates of the error in  $\dot{z}$ , because increasing correlation between errors decreases the effective number of measurements of elevation change for a given region, producing larger errors.

[13] We estimate the on-diagonal covariance at 0.31 m from the  $\hat{\sigma}$  values of crossovers with time differences less than 8 days. Because this period is short, these should contain pass and shot errors but should be essentially unaffected by any elevation change signal. We obtain the off-diagonal covariance,  $\sigma_{pass}$ , by constructing a set of crossovers with essentially no elevation-difference signal correlated between tracks. This amounts to a regression of elevation difference against a model with one independent parameter for each pass across our region, which can be solved by standard methods [Menke, 1989]. Under this regression, the  $\hat{\sigma}$  misfit of eight-day crossovers is 0.26 m; the difference between this and the on-diagonal covariance must be made up by  $\sigma_{pass}$ , so  $\sigma_{pass}$  is  $\sqrt{0.31^2 - 0.26^2}$  m, or about 0.16 m.

[14] Previous measurements of ice elevation change have found seasonal cycles in the elevation of the ice sheet, which are thought to result from seasonal accumulation and from

temperature-dependant densification processes [Zwally and Jun, 2002]. Because we have between 3 and 4 periods of measurements per year, we can estimate the magnitude,  $A$ , and phase,  $\Phi$ , of the dominant elevation-signal. We assume that the  $\Phi$  is spatially uniform, and that  $A$  is proportional to the accumulation rate,  $\dot{b}$ , as estimated by Vaughan *et al.* [1999]. Using all of the cross-overs in our region not eliminated by data-filtering, we fit a model of the form

$$z_a - z_d = \dot{z}(t_a - t_d) + A\dot{b}(\sin(2\pi t_a + \Phi) - \sin(2\pi t_d + \Phi)) \quad (5)$$

to the cross-over differences in a least-squares sense, for  $t$  is in years. The contribution of the seasonal cycle to the cross-over differences is given by equation (5) excluding the secular elevation-rate term. These values may be subtracted from the cross-over values to correct elevation differences for the seasonal cycle.

[15] We also analyze whether constant ranging biases for each period of laser operations could significantly affect the elevation estimates, by estimating the bias for each period by constrained least squares regression. We constrain these biases to have an RMS magnitude of 0.1 m (comparable to the difference between the version 16 and version 18 data releases [Luthcke *et al.*, 2005], and find that the best fitting bias model does not significantly alter the recovered rates of elevation change.

### 3. Results

[16] The data filtering and the 3- $\sigma$  edit leave 19,858 crossovers distributed irregularly over our 28 regions.  $\hat{\sigma}$  residuals for individual regions are between 0.25 and 0.55 m, and the cumulated residuals for all regions have a  $\hat{\sigma}$  of 0.40 m.

[17] Including the seasonal correction reduces the cumulated  $\hat{\sigma}$  residual modestly, to 0.38 m. The best-fitting

seasonal cycle has a minimum on November 15, a maximum on May 15, and an amplitude of 1.9 times the accumulation rate, although shifts in the phase of this cycle by up to 45 days in either direction have little effect on the residuals. The amplitude is mostly determined by measurements during period 2c, because all of the other periods fall near the zero-crossings of the cycle. The mean elevation rate from equation (5) is  $-0.09 \text{ m a}^{-1}$ , which mostly reflects elevation changes on MIS and CIR, near the southern limit of coverage where cross-overs are disproportionately concentrated.

[18] The calculated rates of elevation change, with and without the correction for the seasonal cycle, are given in Table 1 and the elevation rates without the seasonal correction are shown in Figure 1. We only consider significant those rates that are at least twice the formal regression error (typically  $0.02 \text{ m a}^{-1}$ ), and larger than the  $0.07 \text{ m a}^{-1}$  random variation in surface height expected from randomly-varying accumulation and firn density [Wingham, 2000]. Although correcting the data for the seasonal cycle results in a general decrease in the magnitude of elevation rates, only in the VdVIS tributary is the difference significant. In the discussion that follows we will refer to the uncorrected rates.

[19] The largest rates are found in the tributary and junction regions of KIS, where thickening rates are between  $0.25$  and  $0.28 \text{ m a}^{-1}$ . In contrast, the tributary region of WIS and the upstream parts of MIS appear to be thinning: The tributaries of WIS and VdVIS are thinning at  $0.15 \text{ m a}^{-1}$  and  $0.17 \text{ m a}^{-1}$ , respectively, the three divisions of CIR are thinning between  $0.13$  and  $0.18 \text{ m a}^{-1}$ , and the eastern part of MIS is thinning by  $0.05 \text{ m a}^{-1}$ . The downstream portions of MIS are approximately in balance, and the trunk and western portion of WIS appear to be thickening. In the northern part of the embayment, there is strong thinning in the trunk of BIS ( $0.18 \pm 0.03 \text{ m a}^{-1}$ ), with smaller but still significant rates of thinning ( $0.07$ – $0.15 \text{ m a}^{-1}$ ) on MIS, SIR, HIR, and Siple Dome.

#### 4. Discussion

[20] Analysis of ICESat crossover data have provided a new insight into the changes occurring in the RE. The demonstration of known glaciological characteristics of the RE, namely the weak thinning at Siple Dome [Pettit, 2004] and the growth of the upper KIS system [Price et al., 2001], lends credibility to our results. Likewise, comparisons between airborne laser altimetry measurements from 1998 and from 2000, and between these measurements and ICESat, show elevation changes in KIS, VdVIS, and WIS very similar to those we estimate (Csatho et al., submitted manuscript, 2005). However, contrary to our expectation that elevation change should be confined to the ice streams, there appears to be more prevalent surface subsidence: for example, EIR and CIR both show thinning that is stronger than that seen in the adjacent ice streams.

[21] The recovered seasonal cycle is roughly in phase with moisture transport into the RE estimated by Cullather et al. [1998]. This is surprising if the seasonal elevation cycle is due to the accumulation of snow for a constant densification rate, which would imply that the elevation should lag the accumulation, or if the densification is strongest in the summer, which would produce a decrease

in elevation over the summer [Zwally and Jun, 2002]. The recovered seasonal cycle may result from temporally-varying snow density, or may represent an error due to a measurement bias in the laser 2c period. The analysis of further epochs of ICESat data should clarify this.

[22] We do not consider that the prevalent surface lowering is a conclusive indicator of long-term ice-dynamic conditions. It may instead be a result of a deficit in regional accumulation during the study period. Excluding the rapidly-thickening tributaries of KIS and rapidly-thinning CIR, the area-weighted mean elevation change for all regions is  $-0.08 \pm 0.03 \text{ m a}^{-1}$ , which is close to the  $0.07 \text{ m a}^{-1}$  elevation rate variability due to accumulation variations [Wingham, 2000].

[23] Small random accumulation variations cannot explain the rapid thinning of CIR, EIR and HIR. We conclude that this thinning must be a response to recent elevation changes in the ice streams neighboring the ridges. Modeling by Nereson et al. [1998] shows that fast changes in the ice streams are quickly propagated into the ridges, affecting the ridge divide after a delay of about 200 a. The time required for the change in the ridge to reach half of its equilibrium value is longer, about 500 a, so elevation change in the ridges reflects the mean behavior of the ice streams over approximately this period, with increasing sensitivity to recent changes. This thinning in the ridges may reflect retreat of the grounding line: The grounding line appears to have reached its present position at the mouth of MIS relatively recently [Conway et al., 1999], and at WIS it has retreated at an average rate of  $450 \text{ m a}^{-1}$  in the late 20th century [Bindschadler and Vornberger, 1998]. The fact that EIR and CIR are thinning faster than MIS and WIS suggests that rate of thinning in the ice streams was more rapid in the recent past than at present, although the time history of thinning is not possible to resolve from these measurements.

[24] **Acknowledgments.** This work was funded by the NASA Earth Systems Sciences Fellowship, NASA grant NAG5-9906, and the ICESat science team. The authors would like to thank the ICESat science team, Helen Fricker for timely advice on gain corrections, and Howard Conway and Ginny Catania for insights on the history of WAIS, and Robert Bindschadler for editorial advice. We thank NASA's ICESat Science Project and the NSIDC for distribution of the ICESat data, see <http://icesat.gsfc.nasa.gov> and <http://nsidc.org/data/icesat>.

#### References

- Alley, R. B., and R. Bindschadler (2001), The West Antarctic Ice Sheet and sea-level change, in *The West Antarctic Ice Sheet: Behavior and Environment*, *Ant. Res. Ser.*, vol. 77, edited by R. B. Alley and R. A. Bindschadler, pp. 1–12, AGU, Washington, D. C.
- Bentley, C. R. (1987), Antarctic ice streams: A review, *J. Geophys. Res.*, 92, 8843–8868.
- Bindschadler, R., and P. Vornberger (1998), Changes in the West Antarctic Ice Sheet since 1963 from declassified satellite photography, *Science*, 279, 689–692.
- Conway, H., B. L. Hall, G. H. Denton, A. Gades, and E. Waddington (1999), Past and future grounding-line retreat of the West Antarctic Ice Sheet, *Science*, 286, 280–283.
- Cullather, R. J., D. H. Browich, and M. L. Van Woert (1998), Spatial and temporal variability of Anarctic precipitation from atmospheric methods, *J. Clim.*, 11, 334–368.
- Fricker, H. A., A. Borsa, B. Minster, C. Carabajal, K. Quinn, and B. Bills (2005), Assessment of ICESat performance at the salar de Uyuni, Bolivia, *Geophys. Res. Lett.*, 32, L21S06, doi:10.1029/2005GL023423.
- Jezek, K., and RAMP Product Team (2002), RAMP AMM-1 SAR Image Mosaic of Antarctica, <http://nsidc.org/data/nsidc-0103.html>, Alaska SAR Facility, Fairbanks.
- Joughin, I., and S. Tulaczyk (2002), Positive mass balance of the Ross Ice Streams, West Antarctica, *Science*, 295, 476–480.

- Joughin, I., S. Tulaczyk, R. Bindschadler, and S. F. Price (2002), Changes in west Antarctic ice stream velocities: Observation and analysis, *J. Geophys. Res.*, *107*(B11), 2289, doi:10.1029/2001JB001029.
- Luthcke, S. B., D. D. Rowlands, T. A. Williams, and M. Sirota (2005), Reduction of ICESat systematic geolocation errors and the impact on ice sheet elevation change detection, *Geophys. Res. Lett.*, *32*, L21S05, doi:10.1029/2005GL023689.
- Menke, W. (1989), *Geophysical Data Analysis, Discrete Inverse Theory*, *Int. Geophys. Ser.*, vol. 45, Elsevier, New York.
- Nereson, N. A., and C. F. Raymond (2001), The elevation history of the ice streams and spatial accumulation patterns along the Siple Coast of West Antarctica inferred from ground-based radar data from three inter-ice stream ridges, *J. Glaciol.*, *47*, 303–313.
- Nereson, N. A., R. C. A. Hindmarsh, and C. F. Raymond (1998), Sensitivity of the divide position at Siple Dome, West Antarctica, to boundary forcing, *Ann. Glaciol.*, *27*, 207–214.
- Pettit, E. C. (2004), Unique dynamic behaviors of ice divides, Ph.d thesis, Univ. of Wash., Seattle.
- Price, S. F., R. A. Bindschadler, C. L. Hulbe, and I. Joughin (2001), Post-stagnation behavior in the upstream regions of Ice Stream C, West Antarctica, *J. Glaciol.*, *47*, 283–294.
- Spikes, V. B., B. M. Csatho, G. S. Hamilton, and I. M. Whillans (2003), Thickness changes on Whillans Ice Stream and Ice Stream C, West Antarctica, derived from laser altimeter measurements, *J. Glaciol.*, *49*, 223–230.
- Sun, X., J. B. Abshire, and D. Yi (2003), Characteristics and performance of the altimeter receiver, in *Eos Trans. AGU*, *84*(46), Fall Meet. Suppl., Abstract C32A-0432.
- Vaughan, D. J., J. L. Bamber, and M. Giovinetto (1999), Reassessment of net surface mass balance in Antarctica, *J. Clim.*, *12*, 933–946.
- Wingham, D. J. (2000), Short fluctuations in the density and thickness of a dry firn column, *J. Glaciol.*, *146*, 399–411.
- Zwally, H. J., and L. Jun (2002), Seasonal and interannual variations of firn densification and ice-sheet surface elevation at the Greenland summit, *J. Glaciol.*, *48*, 199–207.
- 
- C. R. Bentley, Department of Geology and Geophysics, University of Wisconsin, Madison, WI 53705, USA.
- C. F. Raymond and B. E. Smith, Earth and Space Sciences, University of Washington, Seattle, WA, USA. (ben@ess.washington.edu)